IEEE Access
Multidisciplinary | Rapid Review | Open Access Journal

Received March 18, 2022, accepted April 9, 2022, date of publication April 14, 2022, date of current version April 21, 2022.

Digital Object Identifier 10.1109/ACCESS.2022.3167420

Improved Centroid Algorithm for Beam Stability Control System

HUAN LIU, CHUNYAN WANG, HAO SUN, AND XIAODONG HE
College of Optoelectronic Engineering, Changchun University of Science and Technology, Changchun 130022, China

Corresponding author: Chunyan Wang (985189137@qq.com)

This work was supported by the Key Research and Development Project of Jilin Province Science and Technology Development Plan under Grant 20200401048GX.

ABSTRACT In order to eliminate the beam jitter caused by the air disturbance and the vibrating devices, the error of light spotted jitter must be detected firstly. The beam jitter error can be corrected by a compensator to realize the beam stability control system. In this paper, an Improved Centroid Algorithm (ICA) combining with the Gaussian Fitting Algorithm (GFA), the Bilinear Interpolation and the Weighted Center of Mass (WCOM) was proposed. A Gaussian template is used to roughly locate the spot image in order to improve the efficiency and stability of the algorithm. The light spot image is interpolated by the Bilinear Interpolation to improve the accuracy of centroid identification. The identification accuracy and efficiency of the algorithm were verified by 100 sets of light spot experiments. The experimental results showed that the identification accuracy and efficiency of the Improved Centroid Algorithm were higher than those of the other algorithms. Our algorithm was of great significance for improving the performance of the beam stability control system.

INDEX TERMS Adaptive optics, bilinear interpolation, centroid algorithm, Gaussian fitting.

I. INTRODUCTION

An adaptive optical system is a real time correction system for the wavefront distortion. The beam jitter is the main factor of the wavefront distortion, which has become an urgent problem in the adaptive optical system [1]–[5]. The beam jitter control is important for the beam stability system.

Beam jitter is an external interference, which causes a deflection of the optical axis and resulting in a deviation in the beam propagation direction. In an adaptive optical system, the beam jitter is mainly caused by the atmospheric turbulence, the vibrating devices (such as motors, fans, water coolers, etc.) or the vibration of the optical platform itself [6]–[11]. Therefore, it is necessary to design a beam stability control system to eliminate the beam jitter.

Real-time detection of the centroid is a vital step in the beam stability control system. There are two difficulties with centroid detection. One is to accurately detect the spot and distinguish it from the noise pixel, and the other is to extract the subpixel centroid with a high precision [12]–[15]. At present, the main centroid identification algorithm includes Center of Mass (CoM), the Weighted Center of Mass (WCoM) and Gaussian Fitting Algorithm (GFA), etc. [16]–[23]. Among them, the CoM is suitable for light spot with the small noise and the regular shape. The precision of GFA is high, but the efficiency is low [24], [25].

In this paper, an Improved Centroid Algorithm (ICA) with high accuracy and efficiency is proposed to identify the centroid of light spot. Firstly, the light spot images were filtered by a suitable Gaussian template to determine the rough location of the light spot in the image. After Gaussian filtering, the resolution of the light spot image was increased to the sub-pixel level by the Bilinear Interpolation. And then, the WCoM was used for spot identification to achieve the accurate location. Finally, the accuracy and efficiency of the ICA were verified by the experiments.

II. CENTROIDING ALGORITHMS

A. CENTER OF MASS

In the CoM, the gray value of the target pixel in the light spot area is taken as the weight of its coordinates, and the mean values of the calculated coordinates are the centroid coordinates of the light spot [17], [22], [23], [25]. The centroid is

The associate editor coordinating the review of this manuscript and approving it for publication was Chao Zuo.

calculated referring to (1).

$$\begin{cases} x_0 = \dfrac{\sum_{i=i_1}^{m}\sum_{j=j_1}^{n} f(x_i, y_i) \cdot x_i}{\sum_{i=i_1}^{m}\sum_{j=j_1}^{n} f(x_i, y_i)} \\ y_0 = \dfrac{\sum_{i=i_1}^{m}\sum_{j=j_1}^{n} f(x_i, y_i) \cdot y_i}{\sum_{i=i_1}^{m}\sum_{j=j_1}^{n} f(x_i, y_i)} \end{cases} \tag{1}$$

where (x_0, y_0) is the centroid pixel coordinate, $f(x_i, y_i)$ is the gray value at the grayscale image (x_i, y_i). The algorithm is easy to implement and the identification accuracy is high, but it is sensitive to the pixels outside the peak of the gray graph.

B. WEIGHTED CENTER OF MASS

In order to overcome the limitation of the common centroid algorithm in calculating some special images, the quadratic power of the gray values are used in the WCoM to replace the original gray values for weighting [12], [17], [22].

$$\begin{cases} x_0 = \dfrac{\sum_{i=i_1}^{m}\sum_{j=j_1}^{n} f\,(x_i, y_i)^2 \cdot x_i}{\sum_{i=i_1}^{m}\sum_{j=j_1}^{n} f\,(x_i, y_i)^2} \\ y_0 = \dfrac{\sum_{i=i_1}^{m}\sum_{j=j_1}^{n} f\,(x_i, y_i)^2 \cdot y_i}{\sum_{i=i_1}^{m}\sum_{j=j_1}^{n} f\,(x_i, y_i)^2} \end{cases} \tag{2}$$

However, the WCoM is sensitive to pulse noise, especially when the image quality is poor, its extraction accuracy will decrease sharply.

III. IMPROVED CENTROID ALGORITHM

The ICA is proposed by combining with the GFA, the Bilinear Interpolation and the WCoM. The Gaussian surface approximates to the actual spot with the high stability GFA. The fitted Gaussian surface is discretized and normalized to a (2k + 1) × (2k + 1) light spot template. The image is filtered by the template to reduce the influence of noise on the accuracy of centroid location and simplify the calculation in the centroid identification. At the same time, the spot rough positioning is completed by locating the target spot region in the image. The filtered spot image, is subdivided into the sub-pixel levels by the Bilinear Interpolation to improve the accuracy of the centroid identification. Finally, the WCoM recognizes the interpolated spot image. The algorithm flow is shown in Fig. (1).

A. GENERATING A GAUSSIAN TEMPLATE

The stars image was generated by the off-axis reflection collimator, and the spot images with a large number of star-spots were obtained. Then the light spot is fitted by Gaussian surface to acquire the accurate template. The two-dimensional

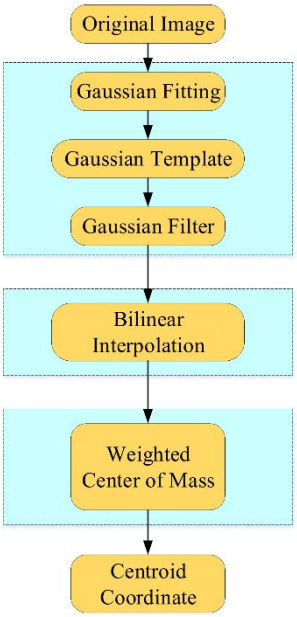

FIGURE 1. Flow chart of improved centroid algorithm.

Gaussian equation is shown in (3):

$$f(x, y) = A \cdot EXP\left[-\frac{(x - x_0)^2}{2\sigma_x^2} - \frac{(y - y_0)^2}{2\sigma_y^2}\right] \tag{3}$$

where A is amplitude, σ_x, σ_y are the standard deviation in the x and y directions respectively. To facilitate calculation, the logarithm on both sides of the Eq. (3) is taken:

$$\ln f = \ln A - \frac{(x - x_0)^2}{2\sigma_x^2} - \frac{(y - y_0)^2}{2\sigma_y^2} \tag{4}$$

Expanding and simplifying (4), t:

$$\ln f = ax^2 + by^2 + cx + dy + m \tag{5}$$

where,

$$\begin{cases} a = -\dfrac{1}{2\sigma_x^2} \\ b = -\dfrac{1}{2\sigma_y^2} \\ c = \dfrac{x_0}{\sigma_x^2} \\ d = \dfrac{y_0}{\sigma_y^2} \\ m = \ln A - \dfrac{x_0^2}{2\sigma_x^2} - \dfrac{y_0^2}{2\sigma_y^2} \end{cases} \tag{6}$$

Using the least square method to minimize the sum of squares of the residuals, we get:

$$Z = \min \sum (ax^2 + by^2 + cx + dy + m - \ln f)^2 \tag{7}$$

0.000023	0.000057	0.000124	0.000235	0.000384	0.000547	0.000676	0.000725	0.000676	0.000547	0.000384	0.000235	0.000124	0.000057	0.000023
0.000057	0.000143	0.000310	0.000584	0.000956	0.001361	0.001682	0.001804	0.001682	0.001361	0.000956	0.000584	0.000310	0.000143	0.000057
0.000124	0.000309	0.000670	0.001264	0.002070	0.002945	0.003639	0.003905	0.003639	0.002945	0.002070	0.001264	0.000670	0.000309	0.000124
0.000233	0.000581	0.001261	0.002377	0.003894	0.005540	0.006846	0.007347	0.006846	0.005540	0.003894	0.002377	0.001261	0.000581	0.000233
0.000381	0.000950	0.002062	0.003887	0.006368	0.009060	0.011195	0.012013	0.011195	0.009060	0.006368	0.003887	0.002062	0.000950	0.000381
0.000541	0.001350	0.002930	0.005524	0.009049	0.012875	0.015909	0.017072	0.015909	0.012875	0.009049	0.005524	0.002930	0.001350	0.000541
0.000668	0.001667	0.003618	0.006821	0.011173	0.015898	0.019644	0.021081	0.019644	0.015898	0.011173	0.006821	0.003618	0.001667	0.000668
0.000717	0.001789	0.003881	0.007318	0.011987	0.017055	0.021075	0.022616	0.021075	0.017055	0.011987	0.007318	0.003881	0.001789	0.000717
0.000668	0.001667	0.003618	0.006821	0.011173	0.015898	0.019644	0.021081	0.019644	0.015898	0.011173	0.006821	0.003618	0.001667	0.000668
0.000541	0.001350	0.002930	0.005524	0.009049	0.012875	0.015909	0.017072	0.015909	0.012875	0.009049	0.005524	0.002930	0.001350	0.000541
0.000381	0.000950	0.002062	0.003887	0.006368	0.009060	0.011195	0.012013	0.011195	0.009060	0.006368	0.003887	0.002062	0.000950	0.000381
0.000233	0.000581	0.001261	0.002377	0.003894	0.005540	0.006846	0.007347	0.006846	0.005540	0.003894	0.002377	0.001261	0.000581	0.000233
0.000124	0.000309	0.000670	0.001264	0.002070	0.002945	0.003639	0.003905	0.003639	0.002945	0.002070	0.001264	0.000670	0.000309	0.000124
0.000057	0.000143	0.000310	0.000584	0.000956	0.001361	0.001682	0.001804	0.001682	0.001361	0.000956	0.000584	0.000310	0.000143	0.000057
0.000023	0.000057	0.000124	0.000235	0.000384	0.000547	0.000676	0.000725	0.000676	0.000547	0.000384	0.000235	0.000124	0.000057	0.000023

FIGURE 2. Gaussian template.

Taking the partial derivative of each variable and setting to zero, the equations are obtained as shown in (8):

$$\begin{cases} \sum (ax^4 + by^2x^2 + cx^3 + dx^2y + mx^2) = \sum x^2 \ln f \\ \sum (ax^2y^2 + by^4 + cxy^2 + dy^3 + my^2) = \sum y^2 \ln f \\ \sum (ax^3 + bxy^2 + cx^2 + dxy + mx) = \sum x \ln f \\ \sum (ax^2y + by^3 + cxy + dy^2 + my) = \sum y \ln f \\ \sum (ax^2 + by^2 + cx + dy + m) = \sum \ln f \end{cases} \tag{8}$$

Then we get the linear equations:

$$BK = C \tag{9}$$

where

$$B = \begin{bmatrix} \sum x^4 & \sum x^2y^2 & \sum x^3 & \sum x^2y & \sum x^2 \\ \sum x^2y^2 & \sum y^4 & \sum xy^2 & \sum y^3 & \sum y^2 \\ \sum x^3 & \sum xy^2 & \sum x^2 & \sum xy & \sum x \\ \sum x^2y & \sum y^3 & \sum xy & \sum y^2 & \sum y \\ \sum x^2 & \sum y^2 & \sum x & \sum y & \sum 1 \end{bmatrix} \tag{10}$$

$$K = \begin{bmatrix} a \\ b \\ c \\ d \\ m \end{bmatrix} \tag{11}$$

and

$$C = \begin{bmatrix} \sum x^2 \ln f \\ \sum y^2 \ln f \\ \sum x \ln f \\ \sum y \ln f \\ \sum \ln f \end{bmatrix} \tag{12}$$

Solving the following equation,

$$K = B^{-1}C \tag{13}$$

The parameter of the Gaussian function can be obtained from the Eq. (6),

$$\begin{cases} x_0 = -\dfrac{c}{2a} \\ y_0 = -\dfrac{d}{2b} \\ \sigma_x = \sqrt{-\dfrac{1}{2d}} \\ \sigma_y = \sqrt{-\dfrac{1}{2m}} \end{cases} \tag{14}$$

Referring to (14), the fitted Gaussian formula can be obtained. The Gaussian discrete template with (x_0, y_0) as the template center expanded to $(2k + 1) \times (2k + 1)$ size. According to the simulation results, the optimal template with $k = 7$ is acquired. And the discrete template is normalized to obtain the 15×15 filtering template, as shown in Fig. 2.

The original image with locating the light spot centroid pixels is smoothed by the Gaussian filter. Then expanding outward the light spot centroid pixels generate a window with a size of 15pixels $\times$ 15pixels for the next steps of the precise positioning. The light spot image after Gaussian filtering is shown in Fig. 3.

B. BILINEAR INTERPOLATION

In order to further improve the centroid identification accuracy, the Bilinear Interpolation is used to interpolate the light spot images (obtained from the rough positioning) to subdivide the pixel into the sub-pixel level [27]. The Bilinear Interpolation algorithm(the first-order interpolation algorithm) can get the final result via three times of the interpolations, which is an improvement to the neighboring interpolation algorithm. In the Bilinear Interpolation algorithm, a first-order Linear Interpolation is performed in the x and y direction. The principle of interpolation is shown in Fig. 4.

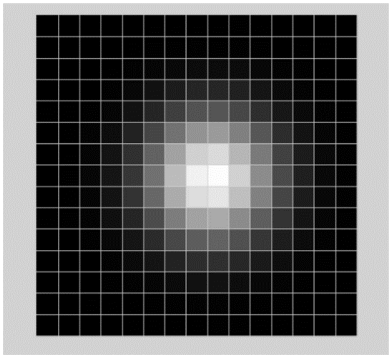

FIGURE 3. The light spot image after Gaussian filtering.

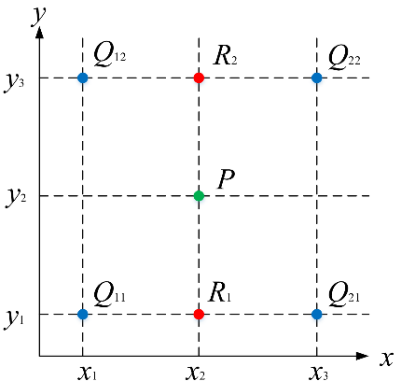

FIGURE 4. The principle of Bilinear Interpolation.

Assume that the coordinate information and grayscale values of the four blue points of $Q_{11}, Q_{12}, Q_{21}, Q_{22}$ in Fig. 3 are given as $Q_{11} = (x_1, y_1)$, $Q_{12} = (x_1, y_3)$, $Q_{21} = (x_3, y_1)$, $Q_{22} = (x_3, y_3)$. Firstly, the gray values of R1 and R2 points are obtained via Linear Interpolation in the x direction. Then the gray values of P point are obtained via Linear Interpolation in the y direction.

The Linear Interpolation in the x direction is written as:

$$\begin{cases} f(R_1) = \dfrac{x_3 - x_2}{x_3 - x_1} f(Q_{11}) + \dfrac{x_2 - x_1}{x_3 - x_1} f(Q_{21}) \\ \qquad \Rightarrow R_1 = (x_2, y_1) \\ f(R_2) = \dfrac{x_3 - x_2}{x_3 - x_1} f(Q_{12}) + \dfrac{x_2 - x_1}{x_3 - x_1} f(Q_{22}) \\ \qquad \Rightarrow R_1 = (x_2, y_2) \end{cases} \tag{15}$$

The Linear Interpolation in the y direction is the following:

$$f(P) = \frac{y_3 - y_2}{y_3 - y_1} f(R_1) + \frac{y_2 - y_1}{y_3 - y_1} f(R_2) \tag{16}$$

Merging (15) and (16),

$$\begin{aligned} f(P) = {} & \frac{(x_3 - x_2)(y_3 - y_2)}{(x_3 - x_1)(y_3 - y_1)} f(Q_{11}) + \frac{(x_2 - x_1)(y_3 - y_2)}{(x_3 - x_1)(y_3 - y_1)} f(Q_{21}) \\ & + \frac{(x_3 - x_2)(y_2 - y_1)}{(x_3 - x_1)(y_3 - y_1)} f(Q_{12}) \\ & + \frac{(x_2 - x_1)(y_2 - y_1)}{(x_3 - x_1)(y_3 - y_1)} f(Q_{22}) \end{aligned} \tag{17}$$

The light spot image after interpolation is shown in Fig. 5.

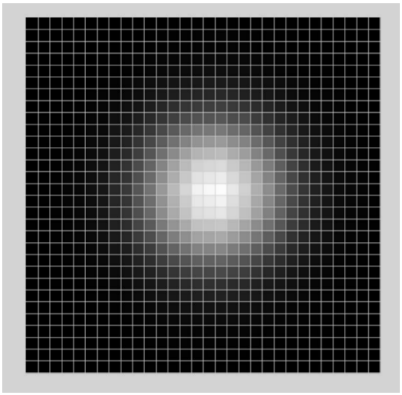

FIGURE 5. The light spot image after interpolation.

Finally, the WCoM recognizes the centroid of the interpolated spot image.

IV. SIMULATION EXPERIMENT

In order to verify the accuracy and efficiency of the proposed ICA algorithm, we simulated 100 Gaussian light spot images and applied to the whole process of light spot centroid identification algorithm. The resolution of the light spot image is 256 pixels × 256 pixels. The gray value of the simulated spot is 0∼255. The different degrees of Gaussian noise are added. The GFA, CoM, WCoM, and ICA are used to identify spot centroid, and the accuracy and efficiency of different algorithms are analyzed and compared. The general Gaussian filter is performed on the image before the GFA, COM, and WCOM identification. The comparison results are shown in from Fig. 6 to Fig. 8, and the datum are shown in Table 1 and Table 2.

From the simulation results, the accuracies of centroid identification for the CoM, WCoM and ICA are high with low noise. Among them, the accuracy of ICA is highest and the centroid identification error of GFA is largest. When the noise is large, the accuracies of the GFA, COM, and WCOM decrease significantly, and the accuracy of ICA is still high and stable. Table 2 shows the calculation time of all centroid algorithms used for a given test image. The calculation speed of the improved ICA is faster than other algorithms.

V. OPTICAL EXPERIMENT

As shown in Fig. 9, the experimental system consists of a lifting platform, a Leica MS60 Electronic Total Station, a plane mirror, sub-arcsec optical axis parallel detection system and an air floating optical platform.

The optical path in the detection system is shown in Fig. 10.

All equipments are built on the air floating optical platform, and the plane mirror is fixed in the Leica MS60 Electronic Total Station, as shown in Fig. 11. The Leica MS60 Electronic Total Station is fixed on the lifting platform and aligned with the optical axis of sub-arcsec optical axis parallel detection system.

In the sub-arcsec optical axis parallel detection system, the light source irradiates on a single star point plate, and the star

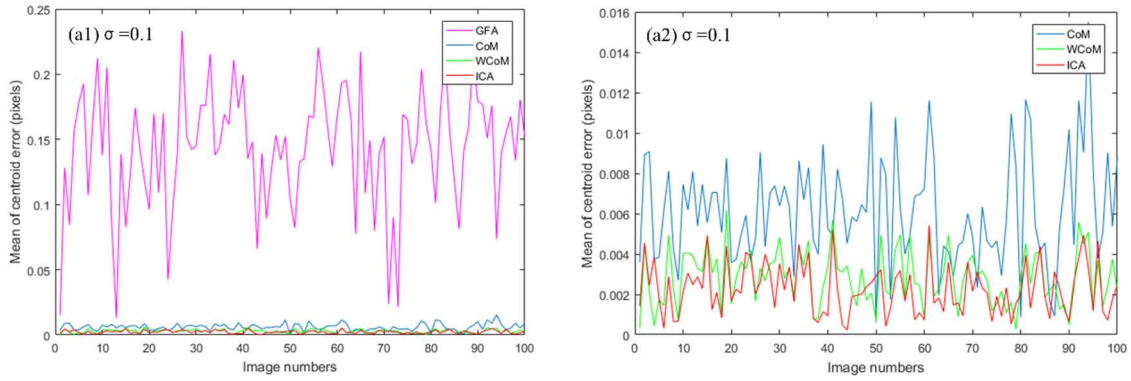

FIGURE 6. (a1) Mean of centroid errors of GFA, CoM, WCoM and ICA when gaussian noise standard deviation $\sigma = 0.1$. (a2) Mean of centroid detection errors of CoM, WCoM and ICA when Gaussian noise standard deviation $\sigma = 0.1$.

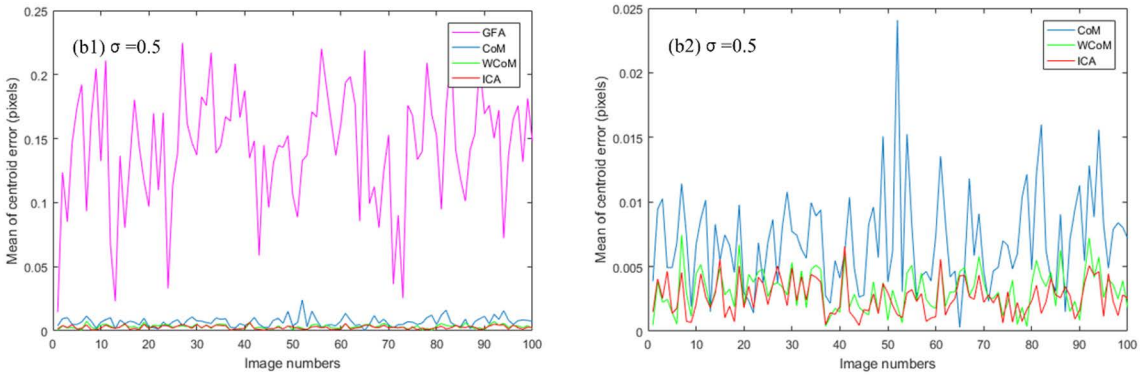

FIGURE 7. (b1) Mean of centroid errors of GFA, CoM, WCoM and ICA when gaussian noise standard deviation $\sigma = 0.5$. (b2) Mean of centroid detection errors of CoM, WCoM and ICA when Gaussian noise standard deviation $\sigma = 0.5$.

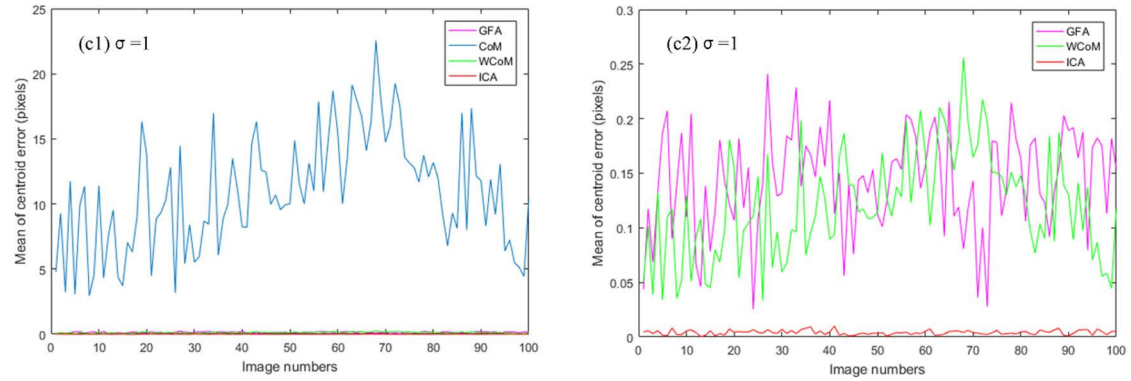

FIGURE 8. (c1) Mean of centroid errors of GFA, CoM, WCoM and ICA when gaussian noise standard deviation $\sigma = 1$. (c2) Mean of centroid detection errors of GFA, WCoM and ICA when Gaussian noise standard deviation $\sigma = 1$.

point target is collimated by an off-axis parabolic reflector, and is reflected by the plane mirror on the electronic total station. The reflective light is incident to the CCD center after passing through the secondary mirror. 100 star point images are collected by the computer, the resolution of the light spot image is 2448 × 2048 pixels. The centroid is identified by four algorithms and the accuracy and efficiency of the centroid identification are compared. Due to the large quantities of acquired images, only 2 of them are listed here, as shown in Fig. 12.

The recognition accuracy of the four algorithms are shown in Fig. 13. The identification accuracy of the ICA algorithm is much higher than that of GFA, CoM and WCoM. There is a slight jitter in the optical path due to the mechanical vibration

TABLE 1. Identification accuracy of different centroid algorithms.

Centroid Algorithm	Error mean of centroid identification under different Gaussian noise (pixels)					
	σ=0.1	σ=0.2	σ=0.3	σ=0.4	σ=0.5	σ=1
GFA	0.14302	0.14302	0.14302	0.14276	0.14280	0.14329
CoM	0.00615	0.00615	0.00611	0.00641	0.00702	10.86901
WCoM	0.00284	0.00284	0.00284	0.00295	0.00317	0.12103
ICA	0.00227	0.00227	0.00228	0.00235	0.00263	0.00411

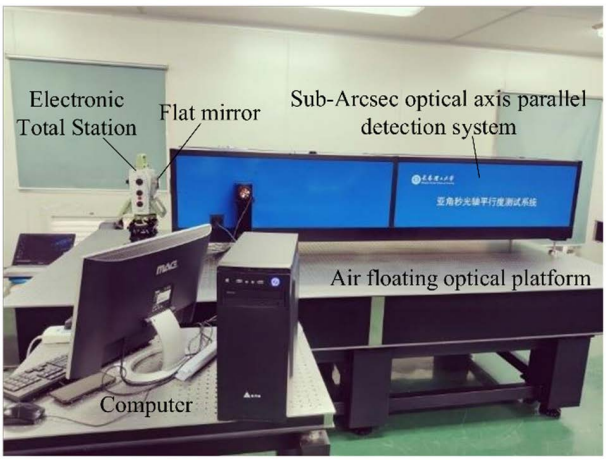

FIGURE 9. The experimental system.

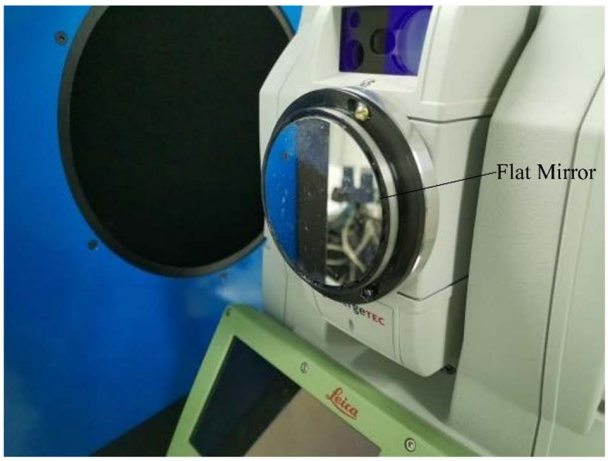

FIGURE 11. Flat mirror is fixed on the Leica MS60 Electronic Total Station.

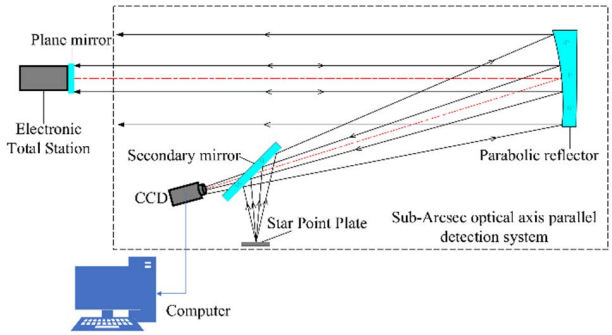

FIGURE 10. Optical path diagram.

FIGURE 12. Star point images.

TABLE 2. Identification efficiency of different algorithms.

Centroid Algorithm	Efficiency (s)
GFA	0.00139
CoM	0.08011
WCoM	0.08019
ICA	0.00120

in the experiment, resulting an increase in the error of the identification accuracy of the centroid, but this does not affect the comparison of the accuracy of the four algorithms.

The computation time of the four algorithms in experimentally acquiring images are listed in table 3. The ICA algorithm is significantly more efficient than the other three algorithms.

Ordinary Gaussian filtering is the process of weighted averaging over the entire image. The value of each pixel is obtained by a weighted average of its own and neighbor pixels. Gaussian filtering is performed by scanning each pixel in the image with a template (or convolution, mask), and replacing the value of the pixel point at the center of the template with the average value. The computation is large.

The calculation efficiency of ICA is higher than other algorithms, because the roughly centroid coordinates (x_0, y_0) is obtained by Gaussian algorithm, i.e., using the Gaussian

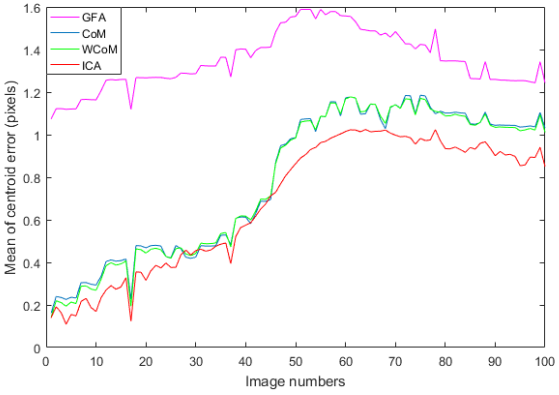

FIGURE 13. Centroid errors of GFA, CoM, WCoM and ICA.

TABLE 3. Identification efficiency of 4 algorithms.

Centroid Algorithm	Efficiency (s)
GFA	0.00269
CoM	5.6801
WCoM	5.7023
ICA	0.00119

discrete template with (x_0, y_0) as the template center and expanding images to 15×15 size. Then the interpolation and centroid identification are directly performed on expanded images, instead of calculating on pixels of the entire image to reduce the amount of calculation, and improve calculation efficiency.

VI. CONCLUSION

In summary, we have proposed an improved centroid algorithm to identify the centroid with high pricision and high efficiency. In the proposed ICA algorithm, the GFA is used to filter the spot image, the light spot images are subdivided into sub-pixel levels by the Bilinear Interpolation, and the WCoM is used for the light spot centroid identification. The experiments demonstrate that the accuracy and efficiency of the ICA algorithm for centroid identification is significantly higher than other algorithms.

There is still a problem in this algorithm, the best Gaussian template cannot be obtained by the calculation. In this paper, according to repeatedly simulation tests, 15×15 template has the best effect. How to calculate the best template needs further research.

ACKNOWLEDGMENT

The authors would like to thank the School of Optoelectronic Engineering, Changchun University of Science and Technology for the cooperation in the experiment. The authors also declare no conflicts of interest in this work or in the publication of this work and also consent to the publication of this work.

REFERENCES

[1] K. Yang, P. Yang, S. Wang, L. Dong, and B. Xu, "Tip-tilt disturbance model identification based on non-linear least squares fitting for linear quadratic Gaussian control," *Opt. Commun.*, vol. 415, pp. 31–38, May 2018.

[2] D. J. Goorskey, J. Schmidt, and M. R. Whiteley, "Efficacy of predictive wavefront control for compensating aero-optical aberrations," *Opt. Eng.*, vol. 52, no. 7, Jul. 2013, Art. no. 071418.

[3] D. C. Frist, "Improved beam jitter control methods for high energy laser systems," Ph.D. dissertation, Dept. Astron. Eng., Naval Postgraduate School, Monterey, CA, USA, 2009.

[4] B. Canuel, E. Genin, M. Mantovani, J. Marque, P. Ruggi, and M. Tacca, "Sub-nanoradiant beam pointing monitoring and stabilization system for controlling input beam jitter in gravitational wave interferometers," *Appl. Opt.*, vol. 53, no. 13, pp. 2906–2916, May 2014.

[5] R. J. Noll, "Zernike polynomials and atmospheric turbulence," *J. Opt. Soc. Amer.*, vol. 66, no. 3, pp. 207–211, Mar. 1976.

[6] P. K. Orzechowski, N. Y. Chen, J. S. Gibson, and T.-C. Tsao, "Optimal suppression of laser beam jitter by high-order RLS adaptive control," *IEEE Trans. Control Syst. Technol.*, vol. 16, no. 2, pp. 255–267, Mar. 2008.

[7] K. J. Yang, P. Yang, S. Chen, S. Wang, L. Wen, L. Dong, X. He, B. Lai, X. Yu, and B. Xu, "Vibration identification based on Levenberg–Marquardt optimization for mitigation in adaptive optics systems," *Appl. Opt.*, vol. 57, no. 11, pp. 2820–2826, Apr. 2018.

[8] J. Garcés, S. Zúñiga, L. M. Close, J. R. Males, K. M. Morzinski, P. Escárate, and M. Castro, "Vibrations in MagAO: Resonance sources identification through frequency-based analysis," *Imag. Appl. Opt.*, Jun. 2015, Art. no. AOTh1D3.

[9] J. R. Maly, D. Erickson, and T. J. Pargett, "Vibration suppression for the Gemini Planet Imager," *Proc. SPIE*, vol. 7733, pp. 77331F-1–77331F-9, Jul. 2010.

[10] Y. Clénet, M. Kasper, N. Ageorges, C. Lidman, T. Fusco, O. P. Marco, M. Hartung, D. Mouillet, B. Koehler, G. Rousset, and N. Hubin, "NAOS performances: Impact of the telescope vibrations and possible origins," *Semaine de L'Astrophysique Francaise*, Dec. 2004, Paper 179.

[11] J. A. Stoesz, J.-P. Veran, F. Rigaut, G. Herriot, L. Jolissaint, and D. Frenette, "Evaluation of the on-sky performance of Altair," *Proc. SPIE*, vol. 5490, pp. 67–78, Oct. 2004.

[12] H. Zhang, Y. Su, J. Shang, L. Yang, B. Cai, C. Liu, J. Wang, S. Zhou, and Z. Zhang, "Accurate star centroid detection for the advanced geosynchronous radiation imager of Fengyun-4A," *IEEE Access*, vol. 6, pp. 7987–7999, 2018.

[13] W. F. Tan, S. Qin, R. M. Myers, T. J. Morris, G. Jiang, Y. Zhao, X. Wang, L. Ma, and D. Dai, "Centroid error compensation method for a star tracker under complex dynamic conditions," *Opt. Exp.*, vol. 25, no. 26, pp. 33559–33574, Dec. 2017.

[14] J. Yan, J. Jiang, and G. Zhang, "Dynamic imaging model and parameter optimization for a star tracker," *Opt. Exp.*, vol. 24, no. 6, pp. 5961–5983, Mar. 2016.

[15] J. Yang, B. Liang, T. Zhang, and J. Song, "A novel systematic error compensation algorithm based on least squares support vector regression for star sensor image centroid estimation," *Sensors*, vol. 11, no. 8, pp. 7341–7363, Jul. 2011.

[16] Z. Wang, J. Jiang, and G. J. Zhang, "Global field-of-view imaging model and parameter optimization for high dynamic star tracker," *Opt. Exp.*, vol. 26, no. 25, pp. 33314–33332, Dec. 2018.

[17] M. V. Arbabmir, S. M. Mohammadi, S. Salahshour, and F. Somayrhee, "Improving night sky star image processing algorithm for star sensors," *J. Opt. Soc. Amer. A, Opt. Image Sci.*, vol. 31, no. 4, pp. 794–801, Apr. 2014.

[18] M. Knutson and D. Miller, "Fast star tracker centroid algorithm for high performance CubeSat with air bearing validation," M.S. thesis, Dept. Astron. Eng., Massachusetts Inst. Technol., Cambridge, MA, USA, 2012.

[19] M. Kolomenkin, S. Pollak, I. Shimshoni, and M. Lindenbaum, "Geometric voting algorithm for star trackers," *IEEE Trans. Aerosp. Electron. Syst.*, vol. 44, no. 2, pp. 441–456, Apr. 2008.

[20] C. Fosu, G. W. Hei, and B. Eissfeller, "Determination of centroid of CCD star images," *Int. Arch. Photogram. Remote Sens. Spatial Inform. Sci.*, vol. 35, pp. 612–617, Jul. 2004.

[21] Z. Dong, X. Sun, F. Xu, and W. Liu, "A low-rank and sparse decomposition-based method of improving the accuracy of sub-pixel grayscale centroid extraction for spot images," *IEEE Sensors J.*, vol. 20, no. 11, pp. 5845–5854, Jun. 2020.

[22] O. Lardière, R. Conan, R. Clare, C. Bradley, and N. Hubin, "Performance comparison of centroiding algorithms for laser guide star wavefront sensing with extremely large telescopes," *Appl. Opt.*, vol. 49, no. 31, p. G78, Nov. 2010.

[23] X. Ji, L. Wang, W.-Y. Sun, and H. Wang, "A k-weighted centroid algorithm based on proximity beacon node optimization," in *Proc. 13th Int. Conf. Natural Comput., Fuzzy Syst. Knowl. Discovery (ICNC-FSKD)*, Jul. 2017, pp. 444–448.
[24] M. Nicolle, T. Fusco, G. Rousset, and V. Michau, "Improvement of Shack–Hartmann wave-front sensor measurement for extreme adaptive optics," *Opt. Lett.*, vol. 29, no. 23, pp. 2743–2745, Dec. 2004.
[25] H. P. Zhang, Y. Su, L. Yang, J. Shang, C. Liu, J. Wang, S. Zhou, Z. Jiang, and Z. Zhang, "Star detection and accurate centroiding for the geosynchronous interferometric infrared sounder of fengyun-4A," *IEEE Access*, vol. 7, pp. 18510–18520, 2019.
[26] S. Y. Pan, S. Wang, J. Xu, L. Fan, F. Yuan, T. Shu, F. Dai, X. Yan, Y. Bu, and X. Wang, "Sub-pixel position estimation algorithm based on Gaussian fitting and sampling theorem interpolation for wafer alignment," *Appl. Opt.*, vol. 60, no. 31, pp. 9607–9617, Nov. 2021.
[27] S. Gao and V. Gruev, "Bilinear and bicubic interpolation methods for division of focal plane polarimeters," *Opt. Exp.*, vol. 19, no. 27, pp. 26161–26173, 2011.

HUAN LIU was born in Changchun, Jilin, China, in 1992. He received the bachelor's and master's degrees in optical engineering from the Changchun University of Science and Technology, in 2015 and 2018, respectively, where he is currently pursuing the Ph.D. degree with the School of Optoelectronic Engineering.

He is the author of four articles and one inventions. His research interests include optical design, adaptive optics, and photoelectric detection.

CHUNYAN WANG was born in Siping, Jilin, China, in 1971. She received the bachelor's and master's degrees from the Changchun Institute of Optics and Fine Mechanics, in 1995 and 2002, respectively, and the Ph.D. degree from the Changchun University of Science and Technology, in 2005.

She became a Professor with the Changchun University of Science and Technology, in 2005. She was a recipient of the one second prize of the National Science and Technology Progress Award; one first prize and two third prizes of the National Defense Science and Technology Progress; one second prize and two third prizes of the Jilin Province Science and Technology Progress Award; five national invention patents; and has published academic more than 40 papers. She is mainly engaged in the research of optical instrument design and testing.

HAO SUN was born in Liaoyuan, Jilin, China, in 1987. She received the bachelor's, master's, and Ph.D. degrees in optical engineering from the Changchun University of Science and Technology, in 2010, 2013, and 2017, respectively.

She is the author of more than ten articles and more than five inventions. Her research interests include optical measurement and precision instrument.

XIAODONG HE was born in Yulin, Shanxi, China, in 1996. He received the B.S. degree in computer science and technology from the Changchun University of Science and Technology, China, in 2015, where he is currently pursuing the M.S. degree in instrument science and technology.

From 2012 to 2015, he used to study computer science and information security. His current research interests include image processing and computer vision.